Pseudoelasticity in FeMnNiAl Shape Memory Alloy lattice structures produced by Laser Powder Bed Fusion

L. Patriarca, W. Abuzaid, G. Carlucci, F. Belelli, R. Casati

Pseudoelasticity in FeMnNiAl Shape Memory Alloy lattice structures produced by Laser Powder Bed Fusion

L. Patriarca[2], W. Abuzaid[1], G. Carlucci[2], F. Belelli[2], R. Casati[2]

[1] American University of Sharjah, Department of Mechanical Engineering, 26666, Sharjah, United Arab Emirates

[2] Politecnico di Milano, Department of Mechanical Engineering, Via La Masa 1, 20156, Milano, Italy

Abstract

This work focusses on microstructure and mechanical properties of FeMnAlNi bulk and micro-lattice structures produced by Laser Powder Bed Fusion, an Additive Manufacturing technology. Microstructure investigation was conducted by means of Electron Back Scattered Electrons analysis, Optical Microscopy and X-Ray Diffraction. The mechanical behavior of the material was evaluated by compression tests and strains were measured by Digital Image Correlation. The material is characterized by coarse grains and by the presence of both austenitic (α-bcc) and martensitic (γ'-fcc) phases. The bulk material recovered an overall and local pseudoelastic strain of 1.3% and 2.9%, respectively. The lattice specimen exhibited ~2% strain recovery.

Additive manufacturing (AM) of shape memory alloys (SMAs), also referred to 4D printing, is positioned to have a major impact on several fields, including aerospace, biomedical, motorsport and construction industries [1]. Historically, most efforts have focused on the NiTi SMA due to its superior shape memory and pseudoealstic (PE) properties [2]. However, and despite the significant advantages of NiTi, the high material cost and relatively low work output levels (due to low strength) limit potential applications [3]. The development of Fe-based SMAs has been motivated by these limitations of NiTi and the need for a cost-effective alternative [3,4]. The FeMnAlNi Fe-based SMA is of

particular interest as it exhibits large levels of PE strains across a wide range of temperatures (about 400K), has significantly higher strength levels compared to NiTi, and a very limited stress dependence (Clausius-Clapeyron slope ≈ 0.5 MPa/K – lowest among all SMA [5]). However, this system possesses significant challenges as it is extremely sensitive to microstructural features (in particular grain size) and requires specifically designed heat treatments to exhibit good functional properties with limited degradation under cyclic loading [4,6].

From an application perspective, engineered micro-lattice systems provide structural properties that are not achievable based solely on the intrinsic properties of materials used in AM [7,8]. Various cell types have been shown to exhibit high structural stiffness and strength levels along with light weight characteristics induced by the hollow/porous design [9–11]. The mechanical performances of such systems can be enhanced through the PE properties of SMAs, which would be very advantageous for the development of high efficiency and light weight structural applications. This work focuses on 4D printing of micro-lattice structures using FeMnAlNi and aims to shed light over functional properties and challenges associated with additive manufacturing.

FeMnAlNi gas atomized powder (+20/-63 µm, D50=29.2 µm) was produced by Nanoval GmbH & Co. KG, Germany. The Renishaw AM250 LPBF system was employed for producing FeMnAlNi lattice and bulk. A 200 W single mode fiber pulsed laser with an estimated beam diameter at focal point of 75 µm was used. Laser melting was performed by discrete and partially overlapped laser spots in a sealed chamber under Ar atmosphere. Hatch distance (h_d=110µm), point distance (p_d=60µm), layer thickness (l=40µm), exposure time (t=80µs), and power (P=200W) were optimized to achieve a maximum relative density of 99.58 %. Samples were produced using a meander scanning strategy and the scanning direction was rotated by 67° after each layer completion. The chemical composition of the as built material is shown in Table 1.

Table 1. Chemical composition of the bulk AM material.

	Fe	Mn	Al	Ni
Bulk (wt.%)	bal.	34.0	8.1	7.0

Two specimen geometries were employed in the present study: compression specimens ($3\times3\times2$ mm^3), and a lattice specimen with a bcc structure (strut diameter of 1.5 mm Figure 1a). This geometry was selected to investigate an AM part designed with thin sub-structures. Prior to testing, all the specimens were heat treated according to the schedule shown in Figure 1b [3,6,12]. Compression tests on the bulk and lattice specimens were conducted in displacement control using a Deben load frame. The axial strains were measured using digital image correlation (DIC).
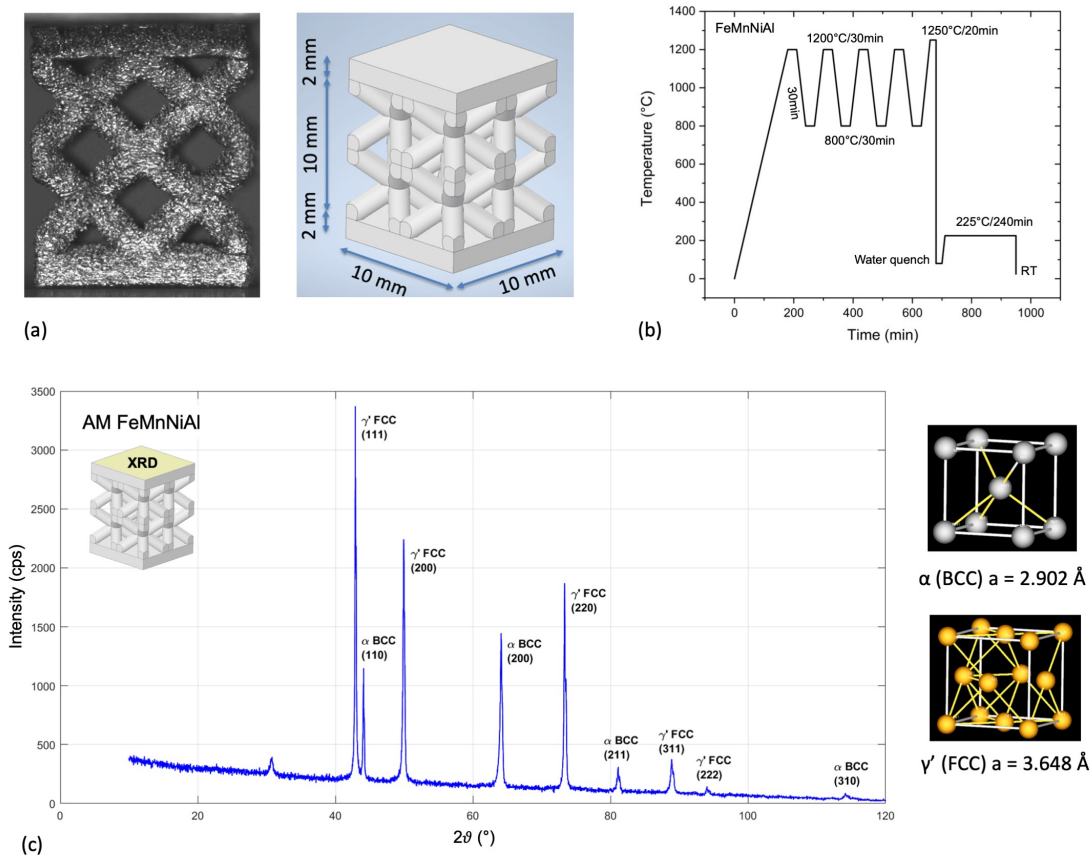

(a)

(b)

(c)

Figure 1. a) Geometry and photograph of the as-built lattice specimen; b) Heat treatment details; c) XRD diffractogram shows reflection peaks of both austenite (α-Fe, bcc) and martensite (γ'-Fe, fcc).

Microstructural observations were conducted with a Nikon Eclipse LV150NL light optical microscope and with Zeiss Sigma 500 field emission scanning electron microscope (FE-SEM), equipped with electron backscattered diffraction detector (EBSD). X-ray diffraction (XRD) experiments were carried out with a Rigaku SmartLab SE multipurpose X-ray diffractometer, which uses copper as a source of radiation with $Cu_{\alpha1}$ of 1.54060 Å and $Cu_{\alpha2}$ of 1.54439 Å operating at 40 kV and 40 mA. The specimen used to perform the XRD analysis was the substrate of the lattice specimen with a dimension of 10mm × 10mm × 1mm. XRD analysis revealed the presence of both austenitic (α-bcc) and martensitic (γ'-fcc) phases, as shown by the diffractogram shown in Figure 1c.

A representative stress-strain plot obtained from a compression test is shown in Figure 2. The DIC maps indicate that the axial strain is not uniform on the specimen surface, and this can be due to differently oriented coarse grains. Therefore, two DIC axial strain measurements were considered, namely i) the overall axial strain of the entire DIC region (*bulk* in Figure 2), ii) the local axial strains of the highly deformed region (*local*). The latter measurement indicates the maximum transformation region detected on the tested sample. A bulk PE strain recovery of 1.3% was measured, whereas the local recovered strain was found to be 2.9%.
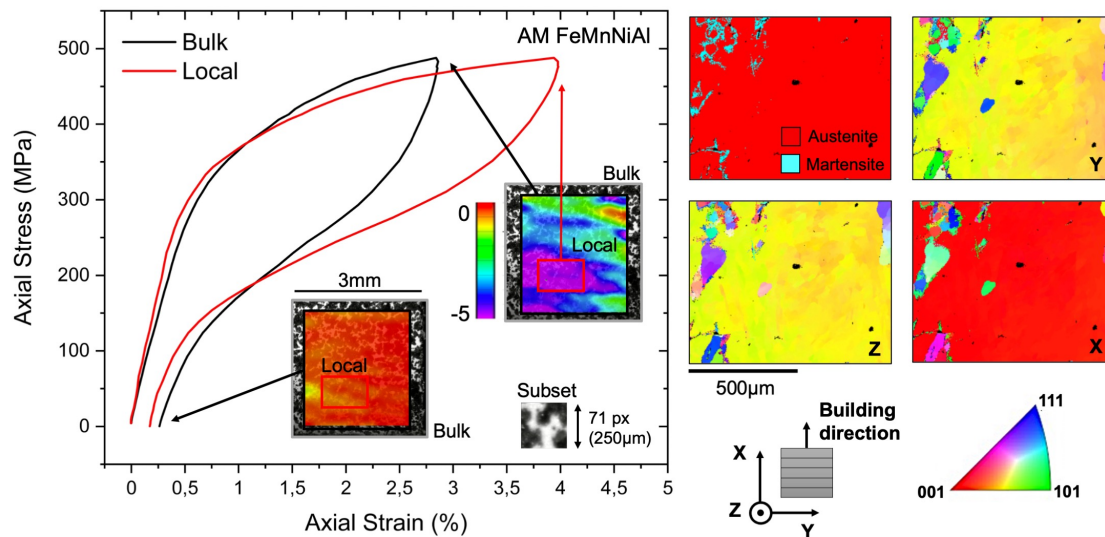

Figure 2. Stress-strain response of an AM FeMnNiAl compression sample. The EBSD maps show the predominance of austenitic phase with a crystal orientation parallel to

<001> along the loading direction. Traces of martensite were observed at the grain boundaries.

The EBSD maps of the region where the local DIC measurements was performed are reported in Figure 2. The top-left phase map shows the presence of both the α and γ' phases, with a clear predominance of the austenitic phase, in good agreement with the PE behavior observed by compression test. The crystal orientation along the loading direction, which also corresponds to the building direction, was the $<001>_\alpha$, as shown by the Inverse Pole Figure (IPF) map labeled as X in Figure 2. This result is in good agreement with the work of Tseng and coworkers [13], in which the authors showed that maximum superelastic strain of 7.2% was measured along the <001> direction of FeMnAlNi single crystal. As noted earlier, the large grain structure, introduced through the cyclic heat treatment, is important for improved PE response in FeMnAlNi [6].

Similar microstructures were also obtained by analyzing the lattice specimen. Figure 3 illustrates the EBSD results for the central region of the lattice structure, at the joint among four struts. The phase map collected by EBSD (Figure 3a) and the optical micrograph (Figure 3b) shows a dual-phase microstructure with austenitic grains that are decorated at boundaries by martensite. γ'-phase was measured to be approximately 10% of volume fraction. The IPF map of Figure 3c indicates the grain boundaries with a black solid line which was defined according to a misorientation angle between grains higher than 10°. In the analyzed area, grains are mainly oriented with the $<111>_\alpha$ parallel to the Y axis (i.e., parallel to the building and loading directions). This microstructure is the result of the adopted heat treatment which induces abnormal grain growth and consequently a predominately coarse grain structure.
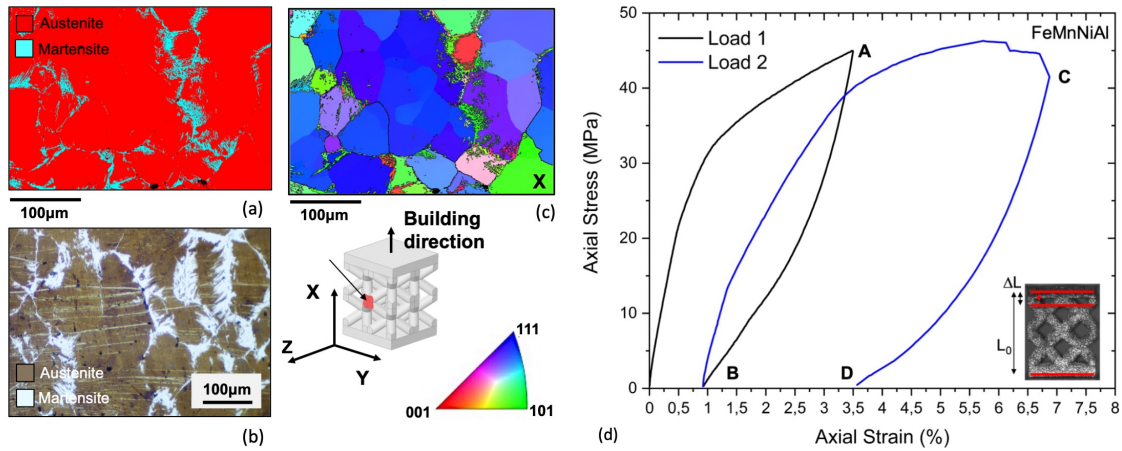
Figure 3. Microstructure of the lattice specimen: a) phase map, b) optical micrograph, c) IPF map; d) Compression test.

The mechanical behavior of the lattice specimen (Figure 3d) was characterized considering the homogenized stress (nominal cross section area of 10×10 mm^2). The axial strain was calculated by means of DIC virtual extensometers as indicated in the schematic of the lattice sample in Figure 3d. After the first mechanical cycle, PE recovered strain of 1.5% was measured following loading to about 3.5% applied strain. In the second loading cycle, the specimen was deformed to 7% strain and the recovery was approximately 2%. To be noted, in the second loading step, the stress-strain curve shows two stress drops due to local fracture in the lattice struts.

As noted in the results in Figure 3d, clear recovery was measured with PE strain recovery reaching up to 2%. It should be noted that the reported results are based on global strain measurements. It is expected that the localized strains are significantly higher with both tensile and compressive magnitudes attributed to the cell design and applied loading (i.e., the struts are subjected to bending). Along with the measured PE response, a finite accumulation of residual strain was also observed, as shown in Figure 3d. The challenges associated with functional degradation of this alloy system and the accumulation of residual martensite, and consequently residual strains, are documented in the literature [14]. However, in the lattice structure considered in this study, the lack of complete recovery is also attributed to small cracks taking place in regions subjected to tensile

loading [15,16]. To reduce cracking in FeMnAlNi, temperature of building platform could be adjusted, as recently shown in [16].

To summarize, the present study illustrates the promising PE properties of the FeMnNiAl SMA manufactured by LPBF. The bulk material recovered an overall PE strain of 1.3% (total recovery ≈ 3%), and a local PE strain of 2.9% along the <001> crystal orientation. The lattice specimen exhibited around 2% strain recovery.

Acknowledgements

References

[1]   J. Gardan, Virtual Phys. Prototyp. 14 (2019) 1–18.

[2]   M. Elahinia, N. Shayesteh Moghaddam, M. Taheri Andani, A. Amerinatanzi, B.A. Bimber, R.F. Hamilton, Prog. Mater. Sci. 83 (2016) 630–663.

[3]   W. Abuzaid, Y. Wu, R. Sidharth, F. Brenne, S. Alkan, M. Vollmer, P. Krooß, T. Niendorf, H. Sehitoglu, Shape Mem. Superelasticity 5 (2019) 263–277.

[4]   T. Omori, K. Ando, M. Okano, X. Xu, Y. Tanaka, I. Ohnuma, R. Kainuma, K. Ishida, Science (80-.). 333 (2011) 68–71.

[5]   J. Xia, Y. Noguchi, X. Xu, T. Odaira, Y. Kimura, M. Nagasako, T. Omori, R. Kainuma, Science (80-.). 369 (2020) 855–858.

[6]   L.W. Tseng, J. Ma, M. Vollmer, P. Krooß, T. Niendorf, I. Karaman, Scr. Mater. 125 (2016) 68–72.

[7]   M.R.K. Ravari, S.N. Esfahani, M.T. Andani, M. Kadkhodaei, A. Ghaei, H. Karaca, M. Elahinia, Smart Mater. Struct. 25 (2016) 025008.

[8]   K.K. Saxena, R. Das, E.P. Calius, Adv. Eng. Mater. 18 (2016) 1847–1870.

[9]   N.A. Fleck, V.S. Deshpande, M.F. Ashby, in: Proc. R. Soc. A Math. Phys. Eng. Sci.,

Royal Society, 2010, pp. 2495–2516.

[10] J.U. Surjadi, L. Gao, H. Du, X. Li, X. Xiong, N.X. Fang, Y. Lu, Adv. Eng. Mater. 21 (2019) 1800864.

[11] F. Rosa, S. Manzoni, R. Casati, Mater. Des. 160 (2018) 1010–1018.

[12] P. La Roca, A. Baruj, C.E. Sobrero, J.A. Malarría, M. Sade, J. Alloys Compd. 708 (2017) 422–427.

[13] L.W. Tseng, J. Ma, Y.I. Chumlyakov, I. Karaman, Scr. Mater. 166 (2019) 48–52.

[14] R. Sidharth, Y. Wu, F. Brenne, W. Abuzaid, H. Sehitoglu, Shape Mem. Superelasticity (2020).

[15] T. Niendorf, F. Brenne, P. Krooß, M. Vollmer, J. Günther, D. Schwarze, H. Biermann, Metall. Mater. Trans. A Phys. Metall. Mater. Sci. 47 (2016) 2569–2573.

[16] F.C. Ewald, F. Brenne, T. Gustmann, M. Vollmer, P. Krooß, T. Niendorf, Metals (Basel). 11 (2021) 185.